Performance Analysis of Distributed Intelligent Reflective Surface Aided Communications

Diluka Loku Galappaththige, Dhanushka Kudathanthirige, and Gayan Amarasuriya
Department of Electrical and Computer Engineering, Southern Illinois University, Carbondale, IL, USA 62901
Email: {diluka.lg, dhanushka.kudathanthirige, gayan.baduge}@siu.edu

***Abstract*—In this paper, the performance of a distributed intelligent reflective surface (IRS)-aided communication system is investigated. To this end, the optimal signal-to-noise ratio (SNR) achievable through the direct and reflected channels is quantified by controlling the phase-shifts of the distributed IRS. This optimal SNR is statistically characterized by deriving tight approximations to the exact probability density function and cumulative distribution function for Nakagami-m fading. Thereby, the outage probability and achievable rate bounds are derived in closed-form, and they are validated via Monte-Carlo simulations. Our numerical results reveal that the distributed IRS-aided communication set-ups can boost the outage and rate performance of wireless systems.**

I. Introduction

Recently, a novel concept of coating physical objects such as building wall and windows within a wireless propagation medium with intelligent reflective surfaces (IRSs), which can interact with electromagnetic (EM) waves, has emerged [1]–[4]. By invoking the recent research developments of meta-surfaces [5]–[7], the feasibility of synthesizing the IRS has been explored [1]. An IRS consists of a large number of passive reflective elements, which can introduce controllable phase-shifts to incident EM waves. These phase-shifts can be intelligently controlled to enable a constructive addition of EM waves at a desired destination and thereby boosting the signal-to-noise ratio (SNR) of the end-to-end communication. Moreover, the IRS enables recycling of EM waves without generating additional signals via radio-frequency (RF) chains/amplifiers and thus enhancing the energy efficiency. Thus, the concept of IRS has a great potential of unveiling a paradigm-shift on how a controllable/smart wireless propagation can be exploited by wireless designers to reach the ultimate performance limits.

Prior related research: In [1], [8], the core architectural aspects of IRSs for wireless communications have been explored. In [5], [6], prototypes of meta-surfaces and meta-tiles that can be used to coat objects embedded within a smart wireless propagation environment have already been developed. In [9], the ray-tracing techniques are used to develop novel propagation/path-loss models for IRS-assisted wireless communications. In [10], [11], the joint optimization of precoders at the base-station and phase-shifts at the IRS is investigated. In [12], the fundamental performance metrics of IRS-assisted communication systems operating over Rayleigh fading are derived. Reference [13] explores the feasibility of exploiting statistical channel state information (CSI) to optimize phase-shift designs at the IRS to maximize the achievable spectral efficiency. In [14], the novel IRS-aided

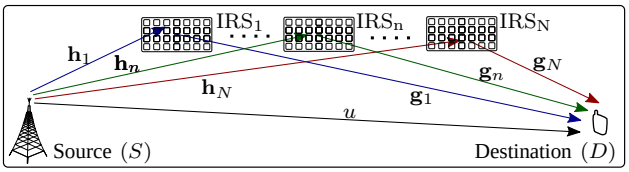

Fig. 1. System model - A distributed IRS-aided communication set-up

techniques are explored to boost the physical layer security aspects of wireless communications. In [15], the performance of IRS-enabled wireless energy harvesting is investigated.

Motivation and our contribution: A common attribute of the above related prior research [1], [5], [6], [8]–[14] is that their system models consist of a single IRS. However, the concept of IRS was originally envisioned to coat physical objects distributed within a wireless propagation channel. To this end, the fundamental performance metrics of a distributed IRS-aided communication set-up have not yet been explored. To fill this important gap in IRS literature, in this paper, we present a statistical characterization of the end-to-end optimal SNR and the corresponding performance metrics of a distributed IRS-aided system operating over Nakagami-m fading. Specifically, the optimal SNR is tightly approximated by using a mathematically tractable counterpart via the central limit theorem because the optimal counterpart does not seem to be amenable to closed-form characterization of the performance metrics. Then, the exact probability density function (PDF) and cumulative distribution function (CDF) of this approximated optimal SNR are derived. Thereby, the outage probability approximation and lower/upper bounds for the achievable rate are derived in closed-form. The accuracy of our analysis is verified via Monte-Carlo simulations, and a set of rigorous numerical results is presented to investigate the performance of the distributed IRS-aided communication system. Our results reveal that a distributed deployment of IRS can be exploited to boost the outage performance and achievable rate compared to the direct transmission and single IRS-aided set-ups.

Notation: $\mathbf{x}^T$ denotes the transpose of $\mathbf{x}$. $\mathbb{E}[X]$ and $\mathbb{V}\mathrm{ar}[X]$ represent the expectation and variance of a random variable (RV) X, respectively. $X \sim \mathcal{N}\left(\mu_X, \sigma_X^2\right)$ denotes that X is Gaussian distributed with μ_X mean and σ_X^2 variance.

II. System, channel and signal models

A. System and channel model

We consider a distributed IRS-assisted communication system in which a single-antenna source (S) serves a single-antenna destination (D) through N distributed IRSs, each

having L passive reflective elements (see Fig. 1). It is assumed that the phase-shifts at the IRS reflective elements can be intelligently controlled such that the received signal at D can be constructively added.

The direct channel between S and D is denoted by u, while the channel between S and the lth reflective element of the nth IRS is represented h_{nl}, respectively. Moreover, g_{nl} is used to denote the channel between the lth reflective element of the nth IRS and D. All channel envelopes are assumed to be independent Nakagami-m distributed, where m is the shape parameter. Nakagami model can capture a wide-range of fading scenarios including Rayleigh, Rician and one-sided Gaussian by varying m. The direct channel (u) can be written in its polar form as

$$u = \alpha_u \mathrm{e}^{j\theta_u}, \tag{1}$$

where α_u is the envelope of u, and θ_u is the phase of u. The PDF of α_u is given by [16]

$$f_{\alpha_u}(x) = \frac{2m_u^{m_u} x^{2m_u-1}}{\Gamma(m_u)\xi_u^{m_u}} \exp\left(\frac{-x^2}{\xi_u}\right), \tag{2}$$

where m_u is the shape parameter, and $\xi_u = m_u\zeta_u$ is the scaling parameter. Here, ζ_u accounts for the large-scale fading/path-loss of the channel. Similarly, the S-to-IRS and IRS-to-D channels can be defined as

$$v_{nl} = \alpha_{v_{nl}} \mathrm{e}^{j\theta_{v_{nl}}}, \tag{3}$$

where $v \in \{h, g\}$. Moreover, $\alpha_{v_{nl}}$ is the envelope of v_{nl}, and $\theta_{v_{nl}}$ is the phase. Then, the PDF of $\alpha_{v_{nl}}$ is given as follows:

$$f_{\alpha_{v_{nl}}}(x) = \frac{2m_v^{m_v} x^{2m_v-1}}{\Gamma(m_v)\xi_{v_n}^{m_v}} \exp\left(\frac{-x^2}{\xi_{v_n}}\right), \tag{4}$$

where $m_{v_{nl}} = m_v$ and $\xi_{v_{nl}} = m_{v_{nl}}\zeta_{v_{nl}} = \xi_{v_n}$ are the shape and scaling parameters, respectively. Here, it is assumed that large-scale fading parameters are the same for a given IRS because its reflective elements are co-located; $\xi_{v_{nl}} = \xi_{v_n}$, $\forall l$. However, ξ_{v_n} depends on the IRS index (n) because geographically distributed IRS deployment.

B. Signal model

The signal transmitted by S reaches at D through the reflected channels of N distributed IRSs and the direct channel. The signal received at D can be written as

$$r = \sqrt{P}\left(u + \sum_{n=1}^{N} \mathbf{g}_n^T \mathbf{\Theta}_n \mathbf{h}_n\right) x + w, \tag{5}$$

where x is the transmitted signal at S satisfying $\mathbb{E}\left[|x|^2\right] = 1$, P is the transmit power, and w is an additive white Gaussian noise (AWGN) at D having zero mean and variance of σ_w^2 such that $w \sim \mathcal{CN}(0, \sigma_w^2)$. In (5), $\mathbf{h}_n = [h_{n1}, \cdots, h_{nl}, \cdots, h_{nL}]^T \in \mathbb{C}^{L\times 1}$ is the channel vector between S and the nth IRS, and $\mathbf{g}_n^T = [g_{n1}, \cdots, g_{nl}, \cdots, g_{nL}] \in \mathbb{C}^{1\times L}$ accounts for the channel vector between the nth IRS and D. Moreover, $\mathbf{\Theta}_n = \mathrm{diag}\left(\eta_{n1}\mathrm{e}^{j\theta_{n1}}, \cdots, \eta_{nl}\mathrm{e}^{j\theta_{nl}}, \cdots, \eta_{nL}\mathrm{e}^{j\theta_{nL}}\right) \in \mathbb{C}^{L\times L}$ is a diagonal matrix, which captures the reflection properties of the nth IRS. Here, $\eta_{nl}\mathrm{e}^{j\theta_{nl}}$ is a complex-valued reflection coefficient at the lth reflective element of the nth IRS, where η_{nl} and θ_{nl} are the magnitude of attenuation and phase-shift, respectively. Thus, the signal received at D in (5) can be rewritten as

$$r = \sqrt{P}\left(u + \sum_{n=1}^{N}\sum_{l=1}^{L} g_{nl}\eta_{nl}\mathrm{e}^{j\theta_{nl}} h_{nl}\right) x + w. \tag{6}$$

The SNR at D can be derived via (6) as

$$\gamma = \bar{\gamma}\left|u + \sum_{n=1}^{N}\sum_{l=1}^{L} g_{nl}\eta_{nl}\mathrm{e}^{j\theta_{nl}} h_{nl}\right|^2, \tag{7}$$

where $\bar{\gamma} = P/\sigma_w^2$ is the transmit SNR. Then, by substituting (1) and (3) into (7), this SNR can be written in terms of the channel phases as

$$\gamma = \bar{\gamma}\left|\alpha_u \mathrm{e}^{j\theta_u} + \sum_{n=1}^{N}\sum_{l=1}^{L} \eta_{nl}\alpha_{g_{nl}}\alpha_{h_{nl}} \mathrm{e}^{j\left(\theta_{nl}+\theta_{g_{nl}}+\theta_{h_{nl}}\right)}\right|^2. \tag{8}$$

This analysis (8) reveals that the received SNR at D can be maximized when NL signal terms inside the summation of (8) are constructively added to the signal component received via the direct channel. By controlling the phase-shifts at each IRS reflective element (θ_{nl}), the phases inside the double summation in (8) can be adjusted to enable a constructive addition of the received signal components via the direct and reflected channels. Thus, the optimal choice of θ_{nl} to maximize the received SNR at D can be given by [10]

$$\theta_{nl}^* = \underset{-\pi\le\theta_{nl}\le\pi}{\mathrm{argmax}}\ \gamma = \theta_u - \left(\theta_{g_{nl}} + \theta_{h_{nl}}\right), \tag{9}$$

for $n \in \{1, \cdots, N\}$ and $l \in \{1, \cdots, L\}$. By using (9), the optimal SNR at D can be derived as

$$\gamma^* = \bar{\gamma}\left[\alpha_u + \sum_{n=1}^{N}\sum_{l=1}^{L} \eta_{nl}\alpha_{g_{nl}}\alpha_{h_{nl}}\right]^2. \tag{10}$$

III. Performance analysis

A. Statistical characterization of the optimal received SNR

The $\alpha_{g_{nl}}$ and $\alpha_{h_{nl}}$ in (10) for $n \in \{1, \cdots, N\}$ and $l \in \{1, \cdots, L\}$ are independently distributed Nakagami random variables, and hence, the exact derivations of the PDFs of

$$Y = \sum_{n=1}^{N}\sum_{l=1}^{L} \eta_{nl}\alpha_{g_{nl}}\alpha_{h_{nl}} \text{ and } \gamma^* = \bar{\gamma}\underbrace{[\alpha_u + Y]}_{R}^2 = \bar{\gamma}R^2, \tag{11}$$

seem mathematically involved and may not provide design insights. Nevertheless, even for moderately large values of the product NL, Y can be tightly approximated by an one-sided Gaussian distributed random variable ($\tilde{Y}$) by invoking the central limit theorem [16]. Then, an approximated PDF for Y can be written as [16] (see Appendix A)

$$f_Y(y) \approx f_{\tilde{Y}}(y) = \begin{cases} \frac{\psi}{\sqrt{2\pi\sigma_Y^2}} \exp\left(-\frac{(y-\mu_Y)^2}{2\sigma_Y^2}\right), & y \ge 0, \\ 0, & y < 0, \end{cases} \tag{12}$$

where $\psi \triangleq 1/\mathcal{Q}\left(-\mu_Y/\sigma_Y\right)$ is a normalization factor to satisfy $\int_{-\infty}^{\infty} f_{\tilde{Y}}(x)dx = 1$, and $\mathcal{Q}(\cdot)$ is the Gaussian-$\mathcal{Q}$ function [16]. In (12), μ_Y and σ_Y^2 can be derived via the moment matching technique as [16] (see Appendix A)

$$\mu_Y = \sum_{n=1}^{N}\sum_{l=1}^{L} \eta_{nl}\sqrt{\frac{\xi_{h_n}\xi_{g_n}}{m_h m_g}} \frac{\Gamma\left(m_h+1/2\right)\Gamma\left(m_g+1/2\right)}{\Gamma\left(m_h\right)\Gamma\left(m_g\right)}, \tag{13a}$$

$$\sigma_Y^2 = \sum_{n=1}^{N}\sum_{l=1}^{L} \eta_{nl}^2\left(\frac{\xi_{h_n}\xi_{g_n}}{m_h m_g}\right) \frac{\Gamma\left(m_h+1\right)\Gamma\left(m_g+1\right)}{\Gamma\left(m_h\right)\Gamma\left(m_g\right)} - \mu_Y^2, \tag{13b}$$

where $\Gamma(t) = \int_0^\infty x^t \mathrm{e}^{-x} dx$ is the Gamma function [17, 8.310.1].

Then, a tight approximation of the PDF of R in (11) or the exact PDF of its approximation $\tilde{R} = \alpha_u + \tilde{Y}$ can be derived as (see Appendix B)

$$f_R(x) \approx f_{\tilde{R}}(x) = \lambda \mathrm{e}^{-\Delta\left(\frac{x-\mu_Y}{2\sigma_Y^2\sqrt{a}}\right)^2} \sum_{k=0}^{2m_u-1} \binom{2m_u-1}{k} \times \left(\frac{x-\mu_Y}{2\sigma_Y^2\sqrt{a}}\right)^{2m_u-1-k} \left[\Gamma\left(\frac{k+1}{2}, \left(\frac{x-\mu_Y}{2\sigma_Y^2\sqrt{a}}\right)^2\right)\right], \quad (14)$$

where $\Gamma(\alpha, x) = \int_x^\infty \mathrm{e}^{-t} t^{\alpha-1} dt$ is the upper incomplete Gamma function [17, 8.350.2]. Here, a, λ, and Δ are

$$a = \frac{m_u}{\xi_u} + \frac{1}{2\sigma_Y^2} \text{ and } \lambda = \frac{m_u^{m_u}\psi}{\Gamma(m_u)\xi_u^{m_u} a^{m_u}\sqrt{2\pi\sigma_Y^2}}, \quad (15a)$$

$$\Delta = \left(\frac{1}{2\sigma_Y^2} - \frac{1}{4a\sigma_Y^4}\right) 4\sigma_Y^4 a. \quad (15b)$$

Thus, an approximation for the PDF of $\gamma^* = \bar{\gamma}R^2$ or the exact PDF of $\gamma^* \approx \tilde{\gamma}^* = \bar{\gamma}\tilde{R}^2$ of can be derived as [16]

$$f_{\gamma^*}(y) \approx f_{\tilde{R}}\left(\sqrt{y/\bar{\gamma}}\right) \times \frac{1}{2\sqrt{\bar{\gamma}y}}. \quad (16)$$

Next, the CDF of $\tilde{R}$ can be derived as (see Appendix C)

$$F_{\tilde{R}}(x) = 1 - \int_x^\infty f_{\tilde{R}}(u)du = 1 - \frac{\lambda}{2a^{m_u}} \sum_{k=0}^{2m_u-1} \binom{2m_u-1}{k} I_k, \quad (17)$$

where I_k is given as

$$I_k = \begin{cases} I_k^o, & \text{odd } k, \\ I_k^e, & \text{even } k. \end{cases} \quad (18)$$

In (18), I_k^o is given by

$$I_k^o = \begin{cases} \frac{q(\gamma_o-1)!}{2} \sum_{i=0}^{\gamma_o-1} \frac{(\Delta+1)^{k/2-m_u-i}}{i!} \left(2\Gamma\left(m_u+i+k/2\right)\right. \\ \left. -\Gamma\left(m_u+i-k/2, (\Delta+1)\, l_{min}^2\right)\right), \text{ for } x < \mu_Y, \\ \frac{q(\gamma_o-1)!}{2} \sum_{i=0}^{\gamma_o-1} \frac{(\Delta+1)^{k/2-m_u-i}}{i!} \\ \times\Gamma\left(m_u+i-k/2, (\Delta+1)\, l_{min}^2\right), \text{ for } x > \mu_Y, \end{cases} \quad (19)$$

where $q = 2\sigma_Y^2\sqrt{a}$, $\gamma_o = (k+1)/2$, and $l_{min} = (x-\mu_Y)/q$. Moreover, I_k^e in (18) can be given as

$$I_k^e = \frac{q(\gamma_e-1)!}{2} \sum_{j=0}^{\gamma_e-1} \frac{\Delta^{j-\gamma_e}}{j!} \left(\Gamma\left(\frac{k+1}{2}, l_{min}^2\right) l_{min}^{2j} \times \exp\left(-\Delta l_{min}^2\right) - \frac{\Gamma\left(j+k/2+1/2, (\Delta+1)l_{min}^2\right)}{(\Delta+1)^{j+k/2+1/2}}\right), \quad (20)$$

where $\gamma_e = m - k/2$. Then, the CDF of $\gamma^* = \bar{\gamma}R^2$ can be approximated as [16]

$$F_{\gamma^*}(y) = \Pr\left(\gamma^* \le y\right) \approx F_{\tilde{R}}\left(\sqrt{y/\bar{\gamma}}\right). \quad (21)$$

Remark 1: The accuracy of the approximated PDF and CDF of γ^* is verified by plotting (16), (21) and the Monte-Carlo simulations of the exact counterparts in Fig. 2 for different N and L. Fig. 2 reveals that our analytical approximations for the PDF (16) and CDF (21) of γ^* are accurate even for moderately large number of reflective elements (L) at the IRS. Since IRSs are typically made of cost-effective reflective elements [18], a moderately large N is practically feasible.

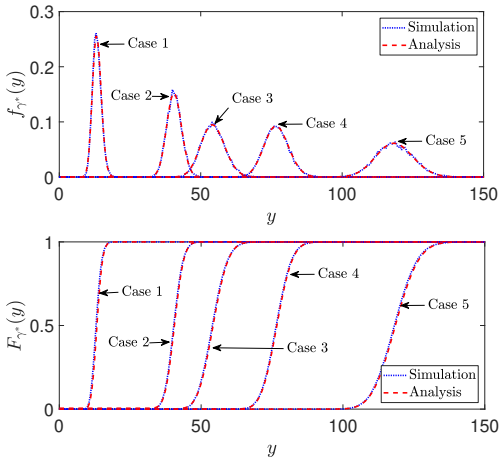

Fig. 2. PDF and CDF of SNR (γ^*) for $\bar{\gamma} = -10$dB. The combinations of N and L for Case 1 to Case 5 are set to $\{N = 2, L = 32\}$, $\{N = 6, L = 32\}$, $\{N = 2, L = 64\}$, $\{N = 8, L = 32\}$, and $\{N = 2, L = 128\}$.

B. Outage probability

The probability that the instantaneous SNR falls below a threshold SNR (γ_{th}) is defined as the SNR outage probability, and a tight approximation to it can be obtained via (21) as

$$P_{out} = P_r\left(\gamma \le \gamma_{th}\right) \approx F_{\gamma^*}(\gamma_{th}). \quad (22)$$

C. Average achievable rate

The average achievable rate can be defined as follows:

$$\mathcal{R} = \mathbb{E}[\log_2\left(1+\gamma^*\right)]. \quad (23)$$

Since the exact derivation of $\mathcal{R}$ in (23) seems mathematically intractable, we resort to tight upper and lower bounds by invoking the Jensens inequality as [19]

$$\mathcal{R}_{lb} \le \mathcal{R} \le \mathcal{R}_{ub}. \quad (24)$$

In (24), $\mathcal{R}_{lb}$ and $\mathcal{R}_{ub}$ are defined as

$$\mathcal{R}_{lb} = \log_2\left(1+\left(\mathbb{E}[1/\gamma^*]\right)^{-1}\right) \approx \log_2\left(1+\left(\mathbb{E}[1/\tilde{\gamma}^*]\right)^{-1}\right), \quad (25a)$$

$$\mathcal{R}_{ub} = \log_2\left(1+\mathbb{E}[\gamma^*]\right) \approx \log_2\left(1+\mathbb{E}[\tilde{\gamma}^*]\right). \quad (25b)$$

The expectation term in (25b) can be approximately derived as (see Appendix D-A)

$$\mathbb{E}[\gamma^*] \approx \mathbb{E}[\tilde{\gamma}^*] = \bar{\gamma}\left(\sigma_u^2 + \sigma_Y^2 + 2\mu_u\mu_Y + \mu_u^2 + \mu_Y^2\right), \quad (26)$$

where μ_Y and σ_Y^2 are defined in (13a) and (13b), respectively. Moreover, μ_u and σ_u^2 are defined as

$$\mu_u = \frac{\Gamma\left(m_u+1/2\right)}{\Gamma\left(m_u\right)} \left(\frac{\xi_u}{m_u}\right)^{1/2}, \quad (27a)$$

$$\sigma_u^2 = \xi_u\left(1 - \frac{1}{m_u}\left(\frac{\Gamma\left(m_u+1/2\right)}{\Gamma\left(m_u\right)}\right)^2\right). \quad (27b)$$

Next, the expectation term in (25a) can be computed as

$$\mathbb{E}[1/\gamma^*] \approx \mathbb{E}[1/\tilde{\gamma}^*] = \frac{1}{\mathbb{E}[\tilde{\gamma}^*]} + \frac{\mathbb{V}\mathrm{ar}[\tilde{\gamma}^*]}{\left(\mathbb{E}[\tilde{\gamma}^*]\right)^3}, \quad (28)$$

where $\mathbb{E}[\tilde{\gamma}^*]$ is defined in (26). Here, $\mathbb{V}\mathrm{ar}[\tilde{\gamma}^*]$ is derived as (see Appendix D-B)

$$\mathbb{V}\mathrm{ar}[\tilde{\gamma}^*] = \bar{\gamma}^2\mathbb{E}\left[\tilde{R}^4\right] - \left(\mathbb{E}[\tilde{\gamma}^*]\right)^2, \quad (29)$$

where $\mathbb{E}\left[\tilde{R}^4\right]$ is given by

$$\mathcal{R}_{lb} = \log_2 \left(1 + \frac{\bar{\gamma} \left(\sigma_u^2 + \sigma_Y^2 + 2\mu_u \mu_Y + \mu_u^2 + \mu_Y^2 \right)^3}{\sum_{n=0}^{4} \binom{4}{n} \frac{\Gamma(m_u + (4-n)/2)}{\Gamma(m_u)} \left(\frac{\xi_u}{m_u} \right)^{(4-n)/2} \frac{\psi}{2\sqrt{\pi}} \sum_{i=0}^{n} \binom{n}{i} \left(2\sigma_Y^2 \right)^{(n-i)/2} \mu_Y^i I\left(n-i, \frac{-\mu_Y}{2\sigma_Y^2} \right)} \right) \tag{34}$$

$$\mathcal{R}_{ub} = \log_2 \left(1 + \bar{\gamma} \left(\sigma_u^2 + \sigma_Y^2 + 2\mu_u \mu_Y + \mu_u^2 + \mu_Y^2 \right) \right) \tag{35}$$

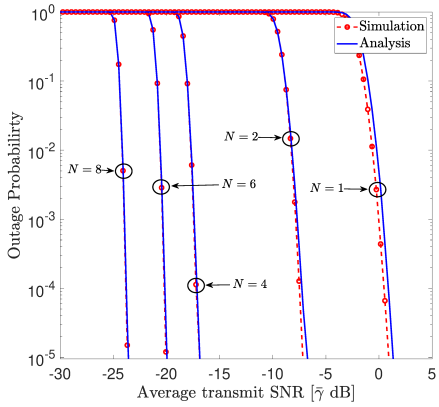

Fig. 3. The outage probability for $N \in \{1, 2, 4, 6, 8\}$, $L = 32$, and $\gamma_{th} = 0$ dB.

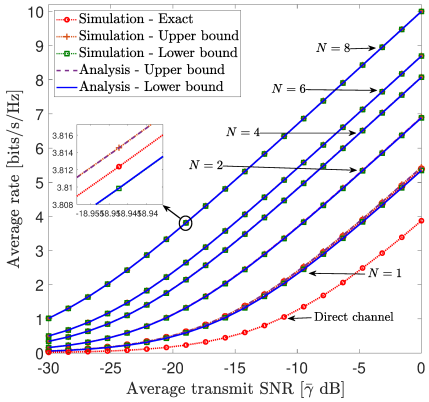

Fig. 4. The average achievable rate for $N \in \{1, 2, 4, 6, 8\}$ and $L = 32$.

$$\mathbb{E}\left[\tilde{R}^4\right] = \sum_{n=0}^{4} \binom{4}{n} \mathbb{E}\left[\alpha_u^{(4-n)}\right] \mathbb{E}\left[\tilde{Y}^n\right]. \tag{30}$$

Here, $\mathbb{E}[\alpha_u^n]$ for $n \in \{1, 2, 3, 4\}$ can be derived as

$$\mathbb{E}[\alpha_u^n] = \frac{\Gamma(m_u + n/2)}{\Gamma(m_u)} \left(\frac{\xi_u}{m_u} \right)^{n/2}. \tag{31}$$

Moreover, $\mathbb{E}\left[\tilde{Y}^n\right]$ for $n \in \{1, 2, 3, 4\}$ is given by

$$\mathbb{E}\left[\tilde{Y}^n\right] = \frac{\psi}{2\sqrt{\pi}} \sum_{i=0}^{n} \binom{n}{i} \left(\sqrt{2\sigma_Y^2} \right)^{n-i} \mu_Y^i I\left(n-i, \frac{-\mu_Y}{2\sigma_Y^2} \right), \tag{32}$$

where $I(\cdot, \cdot)$ is given as

$$I(m,t) = \begin{cases} (-1)^m \gamma\left(\frac{m+1}{2}, t^2\right) + \Gamma\left(\frac{m+1}{2}\right), & \text{for } t \leq 0, \\ \Gamma\left(\frac{m+1}{2}, t^2\right), & \text{otherwise,} \end{cases} \tag{33}$$

where $\gamma(\alpha, x) = \int_0^x \mathrm{e}^{-t} t^{\alpha-1} dt$ is the lower incomplete Gamma function [17, 8.350.1]. Finally, $\mathcal{R}_{lb}$ and $\mathcal{R}_{ub}$ can be derived as (34) and (35), respectively.

IV. Numerical Results

The large-scale fading is modeled as $\zeta_{ab} = (d_0/d_{ab})^{\nu} \times 10^{\varphi_{ab}/10}$, where $a \in \{S, n\}$, $b \in \{n, D\}$, d_{ab} is the distance between nodes a and b, $d_0 = 1\,m$ is a reference distance, $\nu = 2.8$ is the path-loss exponent, and $10^{\varphi_{ab}/10}$ captures log-normal shadow fading with $\varphi_{ab} \sim (0, 8)$ [20]. In the system topology, S and D are in positioned at fixed locations and $1200\,m$ apart from each other. The IRSs are randomly distributed over an area of $1000 \times 2000\,m^2$. Moreover, the amplitude of reflection coefficients η_{nl} for $n \in \{1, \cdots, N\}$ and $l \in \{1, \cdots, L\}$ is set to 0.9, and the Nakagami-m parameters (m_u, m_h, and m_g) are set to 3.

In Fig. 3, the outage probability is plotted as a function of the average transmit SNR ($\bar{\gamma}$) for a distinct set of distributed IRS defined by $N \in \{1, 2, 4, 6, 8\}$. The exact outage curves are generated via Monte-Carlo simulation, while the analytical counterparts are plotted by using our closed-form derivation in (22). Fig. 3 clearly reveals that the tightness of our outage probability approximation significantly improves with N. The distributed IRS deployment outperforms the single-IRS set-up. For instance, to achieve an outage probability of 10^{-4}, the single-IRS set-up requires an average transmit SNR of 1 dB, which is an 104.2% increase compared to the transmit SNR requirement of the distributed deployment with eight IRS.

In Fig. 4, the average achievable rate is plotted for $N \in \{1, 2, 4, 6, 8\}$ and compared it with the rate provided by the direct channel solely. The rate lower/upper bounds are plotted by using (25a) and (25b), respectively, and their accuracy is validated via Monte-Carlo simulation of the exact achievable rate. Fig. 4 clearly depicts that our lower/upper bounds are tight even for smaller N. Fig. 4 reveals that the number of distributed IRS higher the achievable rate. Moreover, Fig. 4 quantifies the achievable rate gains of IRS deployments compared to the direct transmission. For example, at an average transmit SNR of -10 dB, a single-IRS ($N = 1$) case provides a rate gain of 80.7% compared to the direct transmission. Moreover, this rate gain increases to 182.5%, 266.2%, and 405.9% for dual-, quadruple-, and octuple-IRS cases, respectively, with respect to the direct channel.

V. Conclusion

The optimal SNR that is achievable via a distributed IRS-aided communication set-up has been derived and statistically characterized by deriving the tight approximations to the PDF and CDF for Nakagami-m fading. Thereby, the outage probability and achievable rate approximations/bounds have been derived in closed-form. A rigorous set of Monte-Carlo simulations has been presented to validate the accuracy of our

analysis. Our numerical results reveal that distributed IRS setups can be used to significantly enhance the performance of future wireless communications.

APPENDIX A
THE DERIVATION OF μ_Y IN (13a), σ_Y^2 IN (13b), AND PDF OF Y IN (12)

First, we define $Y = \sum_{n=1}^{N}\sum_{l=1}^{L}\eta_{nl}z_{nl}$, where $z_{nl} = \alpha_{h_{nl}}\alpha_{g_{nl}}$. Since $\alpha_{h_{nl}}$ and $\alpha_{g_{nl}}$ are independent Nakagami-m variables, the PDF of z_{nl} can be evaluated as

$$\begin{aligned} f_{z_{nl}}(x) &= \int_0^\infty f_{\alpha_{h_{nl}}}(u) f_{\alpha_{g_{nl}}}(x/u)\times\frac{1}{|u|}du \qquad (36)\\ &= \alpha x^{2m_g-1}\int_0^\infty u^{2(m_h-m_g)-1}\mathrm{e}^{-\frac{m_h u^2}{\xi_{h_n}}-\frac{m_g x^2}{\xi_{g_n}u^2}}du\\ &\overset{(a)}{=} \frac{\alpha}{2}x^{2m_g-1}\int_0^\infty t^{m_h-m_g-1}\mathrm{e}^{-\frac{m_h t}{\xi_{h_n}}-\frac{m_g x^2}{\xi_{g_n}t}}dt\\ &\overset{(b)}{=} \alpha' x^{m_h+m_g-1}\mathcal{K}_{m_h-m_g}\left(2x\sqrt{\frac{m_h m_g}{\xi_{h_n}\xi_{g_n}}}\right), \end{aligned}$$

where $\alpha = 4m_h^{m_h}m_g^{m_g}/\left(\Gamma(m_h)\Gamma(m_g)\xi_{h_n}^{m_h}\xi_{g_n}^{m_g}\right)$ and $\alpha' = \alpha\left(m_g\xi_{h_n}/m_h\xi_{g_n}\right)^{(m_h-m_g)/2}$. Moreover, $\mathcal{K}_v(\cdot)$ is the Modified Bessel function of second kind [17, 8.407]. The step (a) is obtained by letting $t = u^2$, and the step (b) is computed by using [17, 3.471.9]. Then, the nth moment of z_{nl} can be derived as follows:

$$\begin{aligned} \mathbb{E}[z_{nl}^n] &= \alpha'\int_0^\infty x^{m_h+m_g+n-1}\mathcal{K}_{m_h-m_g}\left(2x\sqrt{\frac{m_h m_g}{\xi_{h_n}\xi_{g_n}}}\right)dx \qquad (37)\\ &\overset{(c)}{=} \frac{\alpha'}{4}\left(\frac{m_h m_g}{\xi_{h_n}\xi_{h_n}}\right)^{\frac{-m_h-m_g-n+1}{2}}\Gamma\left(\frac{2m_h+n}{2}\right)\Gamma\left(\frac{2m_g+n}{2}\right), \end{aligned}$$

where the step (c) is written by using [17, 6.561.16]. Then, the mean and the variance of Y can be given as

$$\mu_Y = \mathbb{E}[Y] = \sum_{n=1}^{N}\sum_{l=1}^{L}\eta_{nl}\mathbb{E}[z_{nl}], \qquad (38a)$$

$$\sigma_Y^2 = \mathbb{V}\mathrm{ar}[Y] = \sum_{n=1}^{N}\sum_{l=1}^{L}\eta_{nl}^2\left(\mathbb{E}\left[z_{nl}^2\right]-\mathbb{E}[z_{nl}]^2\right). \qquad (38b)$$

By substituting (37) into (38a) and (38b), μ_Y and σ_Y can be computed as (13a) and (13b), respectively. Then, the PDF of Y can be approximated by an one-sided Gaussian distribution as given in (12) by invoking the central limit theorem [16].

APPENDIX B
THE DERIVATION OF PDF OF $\tilde{R}$ IN (14)

Since α_u and Y are independent random variables, the PDF of $\tilde{R} = \alpha_u + \tilde{Y}$ can be derived as follows:

$$\begin{aligned} f_{\tilde{R}}(x) &= \int_0^\infty f_u(u) f_{\tilde{Y}}(x-u)du \qquad (39)\\ &= 2a^{m_u}\lambda\mathrm{e}^{-\frac{(x-\mu_Y)^2}{2\sigma_Y^2}}\int_0^\infty u^{2m_u-1}\mathrm{e}^{-au^2+bu}du\\ &= 2a^{m_u}\lambda\mathrm{e}^{-\frac{(x-\mu_Y)^2}{2\sigma_Y^2}}\mathrm{e}^{\frac{b^2}{4a}}\underbrace{\int_0^\infty u^{2m_u-1}\mathrm{e}^{-a\left(u-\frac{b}{2\sqrt{a}}\right)^2}du}_{I_{\tilde{R}}}, \end{aligned}$$

where $b = (x-\mu_Y)/\sigma_Y^2$. Here, a and λ are defined in (15a) and (15a), respectively. The solution to (39) is given by

$$\begin{aligned} I_{\tilde{R}} &= \frac{1}{a^{m_u}}\int_{\frac{-b}{2\sqrt{a}}}^\infty\left(t+\frac{b}{2\sqrt{a}}\right)^{2m_u-1}\mathrm{e}^{-t^2}dt \qquad (40)\\ &= \frac{1}{a^{m_u}}\sum_{k=0}^{2m_u-1}\binom{2m_u-1}{k}\left(\frac{b}{2\sqrt{a}}\right)^{2m_u-1-k}\int_{\frac{-b}{2\sqrt{a}}}^\infty t^k\mathrm{e}^{-t^2}dt\\ &\overset{(d)}{=} \frac{1}{2a^{m_u}}\sum_{k=0}^{2m_u-1}\binom{2m_u-1}{k}\left(\frac{b}{2\sqrt{a}}\right)^{2m_u-1-k}\Gamma\left(\frac{k+1}{2},\frac{b^2}{4a}\right), \end{aligned}$$

where the step (d) is due to [17, 2.33.10]. By substituting (b) and (40) into (39), the PDF of $\tilde{R}$ is derived as (14).

APPENDIX C
THE DERIVATION OF CDF OF $\tilde{R}$ IN (17)

By substituting (14) into (17), I_k in (17) can be given as

$$\begin{aligned} I_k &= \int_x^\infty \mathrm{e}^{-\Delta\left(\frac{u-\mu_Y}{q}\right)^2}\left(\frac{u-\mu_Y}{q}\right)^{2m_u-1-k}\Gamma\left(\frac{k+1}{2},\left(\frac{u-\mu_Y}{q}\right)^2\right)du\\ &\overset{(e)}{=} q\int_{l_{min}}^\infty \mathrm{e}^{-\Delta t^2}t^{2m_u-1-k}\Gamma\left(\frac{k+1}{2},t^2\right)dt, \qquad (41) \end{aligned}$$

where $q = 2\sigma_Y^2\sqrt{a}$, $l_{min} = (x-\mu_Y)/q$, and the step (e) is written by changing the variable of integration. Then, we divide I_k into two integrals: (i) I_k^o for odd values of k and (ii) I_k^e for even values of k. Thus, for odd values of k and when $x-\mu_Y < 0$, this integral can be written as

$$\begin{aligned} I_k^o = q\underbrace{\int_{l_{min}}^0 \mathrm{e}^{-\Delta t^2}t^{2m_u-1-k}\Gamma\left(\frac{k+1}{2},t^2\right)dt}_{I_{k1}^o}\\ +q\underbrace{\int_0^\infty \mathrm{e}^{-\Delta t^2}t^{2m_u-1-k}\Gamma\left(\frac{k+1}{2},t^2\right)dt}_{I_{k2}^o}. \qquad (42) \end{aligned}$$

Then, the first integral I_{k1}^o in (42) can be computed as

$$\begin{aligned} I_{k1}^o &\overset{(f)}{=} \int_0^{-l_{min}}\mathrm{e}^{-\Delta y^2}y^{2m_u-1-k}\Gamma\left(\frac{k+1}{2},y^2\right)dy \qquad (43)\\ &\overset{(g)}{=} (\gamma_o-1)!\sum_{i=0}^{\gamma_o-1}\frac{1}{i!}\int_0^{-l_{min}}\mathrm{e}^{-(\Delta+1)y^2}y^{2m_u-1-k}dy\\ &\overset{(h)}{=} \frac{(\gamma_o-1)!}{2}\sum_{i=0}^{\gamma_o-1}\frac{(\Delta+1)^{k/2-m_u-i}}{i!}\int_0^{l_{min}^2(\Delta+1)}v^{m_u+i-k/2}\mathrm{e}^{-v}dv\\ &\overset{(i)}{=} \frac{(\gamma_o-1)!}{2}\sum_{i=0}^{\gamma_o-1}\frac{(\Delta+1)^{k/2-m_u-i}}{i!}\gamma\left(m_u+i-\frac{k}{2},(\Delta+1)l_{min}^2\right), \end{aligned}$$

where the step (f) and step (h) are obtained by substituting $t = -y$ and $v = (\Delta+1)y^2$, respectively. The step (g) is computed via the fact that $\Gamma(n,x) = (n-1)!\mathrm{e}^{-x}\sum_{m=0}^{n-1}x^m/m!$ [17, 8.352.7]. The step (i) is written by using [17, 8.350.1]. The second integral I_{k2}^o in (42) can be computed as

$$\begin{aligned} I_{k2}^o &= \int_0^\infty \mathrm{e}^{-\Delta t^2}t^{2m_u-1-k}\Gamma\left(\frac{k+1}{2},t^2\right)dt \qquad (44)\\ &\overset{(j)}{=} (\gamma_o-1)!\sum_{i=0}^{\gamma_o-1}\frac{1}{i!}\int_0^\infty t^{2m_u+2i-1-k}\mathrm{e}^{-(\Delta+1)t^2}dt\\ &\overset{(k)}{=} \frac{(\gamma_o-1)!}{2}\sum_{i=0}^{\gamma_o-1}\frac{(\Delta+1)^{k/2-m_u-i}}{i!}\Gamma\left(m_u+i-\frac{k}{2}\right), \end{aligned}$$

where the step (j) is derived via a similar technique used in the step (g), and the step (k) is evaluated by using [17, 2.33.10]. Then, for $x-\mu_Y>0$, I_k^o can be calculated as

$$\begin{aligned} I_k^o &= \int_{l_{min}}^{\infty} \mathrm{e}^{-\Delta t^2} t^{2m_u-1-k}\Gamma\left(\frac{k+1}{2},t^2\right)dt \qquad (45)\\ &= (\gamma_o-1)!\sum_{i=0}^{\gamma_o-1}\frac{1}{i!}\int_{l_{min}}^{\infty} t^{2m_u+2i-1-k}\mathrm{e}^{-(\Delta+1)t^2}dt \\ &= \frac{(\gamma_o-1)!}{2}\sum_{i=0}^{\gamma_o-1}\frac{(\Delta+1)^{k/2-m_u-i}}{i!}\Gamma\left(m_u+i-\frac{k}{2},(\Delta+1)l_{min}^2\right). \end{aligned}$$

By combining (42) and (45), I_k^o can be derived as (19). Then, for even values of k, the integral in (41) can be evaluated as

$$\begin{aligned} I_k^e &= q\int_{l_{min}}^{\infty} \mathrm{e}^{-\Delta t^2} t^{2m_u-1-k}\Gamma\left(\frac{k+1}{2},t^2\right)dt \qquad (46)\\ &\overset{(l)}{=} \frac{(\gamma_e-1)!}{2}\sum_{j=0}^{\gamma_e-1}\left[-\frac{\mathrm{e}^{-\Delta t^2}t^{2j}}{j!\Delta^{\gamma_e-1}}\Gamma\left(\frac{k+1}{2},t^2\right)\right]_{l_{min}}^{\infty} \\ &\quad -(\gamma_e-1)!\sum_{j=0}^{\gamma_e-1}\frac{\Delta^{\gamma_e-1}}{j!}\int_{l_{min}}^{\infty} t^{k+2j}\mathrm{e}^{-(\Delta-1)t^2}dt \\ &= \frac{(\gamma_e-1)!}{2}\sum_{j=0}^{\gamma_e-1}\frac{\mathrm{e}^{-\Delta l_{min}^2}l_{min}^{2j}}{j!\Delta^{\gamma_e-1}}\Gamma\left(\frac{k+1}{2},l_{min}^2\right) \\ &\quad -\frac{(\gamma_e-1)!}{2}\sum_{j=0}^{\gamma_e-1}\frac{\Delta^{\gamma_e-1}}{j!}\frac{\Gamma\left(j+\frac{k}{2}+\frac{1}{2},(\Delta+1)l_{min}^2\right)}{(\Delta+1)^{j+k/2+1/2}}, \end{aligned}$$

where the step (l) is obtained by using the part-by-part integration technique.

APPENDIX D

A. The derivation of expectation of $\tilde{\gamma}^*$ in (26)

The expectation term in (26) can be computed as

$$\begin{aligned} \mathbb{E}[\tilde{\gamma}^*] &= \mathbb{E}\left[\bar{\gamma}\tilde{R}^2\right] = \bar{\gamma}\mathbb{E}\left[(\alpha_u+\tilde{Y})^2\right] = \bar{\gamma}\sum_{n=0}^{2}\binom{2}{n}\mathbb{E}\left[\alpha_u^{(2-n)}\right]\mathbb{E}\left[\tilde{Y}^n\right] \\ &= \bar{\gamma}\left(\sigma_u^2+\mu_u^2+\sigma_Y^2+\mu_Y^2+2\mu_u\mu_Y\right), \qquad (47) \end{aligned}$$

where μ_Y, σ_Y^2, μ_u, and σ_u^2 are given in (13a), (13b), (27a), and (27b), receptively.

B. The derivation of variance of $\tilde{\gamma}^*$ in (29)

The first expectation term in (29) can be evaluated as

$$\mathbb{E}\left[\tilde{R}^4\right] = \mathbb{E}\left[(\alpha_u+\tilde{Y})^4\right] = \sum_{n=0}^{4}\binom{4}{n}\mathbb{E}\left[\alpha_u^{(4-n)}\right]\mathbb{E}\left[\tilde{Y}^n\right]. \qquad (48)$$

Thus, the nth moment of α_u^n denoted by $\mathbb{E}[\alpha_u^n]$ can be computed as

$$\begin{aligned} \mathbb{E}[\alpha_u^n] &= \int_0^{\infty} x^n f_u(x)dx \qquad (49)\\ &= \frac{2m_u^{m_u}}{\Gamma(m_u)\xi_u^{m_u}}\int_0^{\infty} x^{2m_u+n-1}\mathrm{e}^{-\frac{m_u x^2}{\xi_u}}dx \\ &\overset{(m)}{=} \frac{\xi_u^{n/2}}{\Gamma(m_u)m_u^{n/2}}\Gamma\left(m_u+n/2\right), \end{aligned}$$

where the step (m) is evaluated by using [17, 2.33.10]. Then, $\mathbb{E}\left[\tilde{Y}^n\right]$ can be derived as

$$\begin{aligned} \mathbb{E}\left[\tilde{Y}^n\right] &= \frac{\psi}{\sqrt{2\pi\sigma_Y^2}}\int_0^{\infty} y^n\mathrm{e}^{-\frac{(y-\mu_Y)^2}{2\sigma_Y^2}}dy \qquad (50)\\ &\overset{(n)}{=} \frac{\psi}{\sqrt{\pi}}\int_{\frac{-\mu_Y}{\sqrt{2\sigma_Y^2}}}^{\infty}\left(\sqrt{2\sigma_Y^2}t+\mu_Y\right)^n\mathrm{e}^{-t^2}dt \\ &\overset{(o)}{=} \frac{\psi}{2\sqrt{\pi}}\sum_{i=0}^{n}\binom{n}{i}\left(\sqrt{2\sigma_Y^2}\right)^{n-i}\mu_Y^i I\left(n-i,\frac{-\mu_Y}{2\sigma_Y^2}\right), \end{aligned}$$

where the step (n) is due to a changing of variable, and the step (o) is obtained by expanding $\left(\sqrt{2\sigma_Y^2}t+\mu_Y\right)^n$ based on n value. Moreover, $I(\cdot,\cdot)$ is given in (33).

REFERENCES

[1] C. Liaskos *et al.*, "A New wireless Communication Paradigm through Software-Controlled Metasurfaces," *IEEE Commun. Mag.*, vol. 56, no. 9, pp. 162–169, 2018.

[2] M. Di Renzo et al., "Smart Radio Environments Empowered by Reconfigurable AI Meta-Surfaces: An idea whose time has come," *EURASIP J. Wireless Commun. Net.*, May 2019.

[3] H. Yang et al., "A Programmable Metasurface with Dynamic Polarization, Scattering and Focusing Control," *Scientific Reports*, vol. 6, 2016.

[4] J. Su et al., "Ultrawideband, Wide Angle and Polarization-in-Sensitive Specular Reflection Reduction by Metasurface Based on Parameter-Adjustable Meta-Atoms," *Scientific Reports*, vol. 7, 2017.

[5] S. H. Lee et al., "Switching Terahertz Waves with Gate-Controlled Active Graphene Metamaterials," *Nature Materials*, vol. 11, no. 11, p. 936?41, 2012.

[6] T. Sekitani et al., "Stretchable Active-Matrix Organic Light-Emitting Diode Display Using Printable Elastic Conductors," *Nature Materials*, vol. 11, no. 11, p. 494?99, 2009.

[7] T. J. Cui *et al.*, "Coding Metamaterials, Digital Metamaterials and Programmable Metamaterials," *Light: Science and Applications*, vol. 3, no. 10, Oct. 2014.

[8] Liaskos et al., "Design and Development of Software Defined Metamaterials for Nanonetworks," *IEEE Circuits Syst. Mag.*, vol. 15, no. 4, pp. 12–25, 2015.

[9] E. Basar *et al.*, "Wireless Communications Through Reconfigurable Intelligent Surfaces," vol. 7, pp. 116 753–116 773, 2019.

[10] Q. Wu and R. Zhang, "Intelligent Reflecting Surface Enhanced Wireless Network via Joint Active and Passive Beamforming," *IEEE Trans. Wireless Commun.*, pp. 1–1, 2019.

[11] ——, "Beamforming Optimization for Wireless Network Aided by Intelligent Reflecting Surface with Discrete Phase Shifts," *IEEE Trans. Commun.*, vol. 68, no. 3, pp. 1838–1851, 2020.

[12] D. Kudathanthirige, D. Gunasinghe, and G. Amarasuriya, "Performance Analysis of Intelligent Reflective Surfaces for Wireless Communication," *arXiv e-prints*, Feb. 2020.

[13] Y. Han *et al.*, "Large Intelligent Surface-Assisted Wireless Communication Exploiting Statistical CSI," *IEEE Trans. Veh. Technol.*, vol. 68, no. 8, pp. 8238–8242, Aug 2019.

[14] J. Chen *et al.*, "Intelligent Reflecting Surface: A Programmable Wireless Environment for Physical Layer Security," vol. 7, pp. 82 599–82 612, 2019.

[15] Q. Wu and R. Zhang, "Weighted Sum Power Maximization for Intelligent Reflecting Surface Aided SWIPT," vol. 9, no. 5, pp. 586–590, 2020.

[16] A. Papoulis and S. U. Pillai, *Probability, Random Variables, and Stochastic Processes*, 4th ed. McGraw Hill, 2002.

[17] I. Gradshteyn and I. Ryzhik, *Table of Integrals, Series, and Products*, 7th ed. Academic Press, 2007.

[18] Q. Wu and R. Zhang, "Towards Smart and Reconfigurable Environment: Intelligent Reflecting Surface Aided Wireless Network," *IEEE Commun. Mag.*, vol. 58, no. 1, pp. 106–112, 2020.

[19] Q. Zhang *et al.*, "Power Scaling of Uplink Massive MIMO Systems with Arbitrary-Rank Channel Means," *IEEE J. Sel. Areas Signal Process.*, vol. 8, no. 5, pp. 966–981, Oct. 2014.

[20] T. L. Marzetta *et al.*, *Fundamentals of Massive MIMO*. Cambridge University Press, Cambridge, UK, 2016.